Structure of Human Pro-Matrix Metalloproteinase-2: Activation Mechanism Revealed

Ekaterina Morgunova,[1,2] Ari Tuuttila,[1] Ulrich Bergmann,[1] Mikhail Isupov,[3] Ylva Lindqvist,[2] Gunter Schneider,[2]* Karl Tryggvason[1]*

Matrix metalloproteinases (MMPs) catalyze extracellular matrix degradation. Control of their activity is a promising target for therapy of diseases characterized by abnormal connective tissue turnover. MMPs are expressed as latent proenzymes that are activated by proteolytic cleavage that triggers a conformational change in the propeptide (cysteine switch). The structure of proMMP-2 reveals how the propeptide shields the catalytic cleft and that the cysteine switch may operate through cleavage of loops essential for propeptide stability.

Matrix metalloproteinases (MMPs) are key enzymes involved in connective tissue turnover in normal and pathological conditions (*1*). MMPs exist in both invertebrate and vertebrate species. In vertebrates, they are expressed mainly in connective tissue cells and in cells of bone marrow origin. MMPs are extracellular enzymes [except for the membrane-type MMPs (MT-MMPs)] that are secreted as proenzymes. Their activity is controlled by transcriptional regulation, zymogen activation, and specific tissue inhibitors of metalloproteinases (TIMPs) (*1, 2*).

MMP-2 and MMP-9 degrade type IV collagen, the major component of basement membranes and denatured collagen (gelatin) (*1, 2*). MMP-2 is primarily expressed in mesenchymal cells (mainly fibroblasts) during development and tissue regeneration. It was originally isolated from a malignant mouse tumor and was found to be highly expressed in stromal cells surrounding the invading front of metastasizing tumors (*3*). This indicated that type IV collagenolytic activity is required by metastasizing tumor cells to traverse basement membranes at tissue boundaries and in blood vessels. Therefore, these enzymes are a promising target for the development of antitumor drugs.

All the MMPs are multidomain enzymes containing propeptide, catalytic, and hemopexin (except matrilysin, MMP-7) domains. Additionally, MMP-2 and MMP-9 contain three contiguous fibronectin type II-like domains that are inserted within their catalytic domain. A cysteine residue, strictly conserved in the propeptide domain of all MMPs, has been shown to be essential for maintaining the MMPs in an inactive state (*2, 4*). It has been suggested that the sulfhydryl group of this cysteine residue is coordinated to the catalytic Zn^{2+} ion and that interruption of this interaction causes activation [cysteine-switch mechanism (*4*)]. Physiologic activation of MMPs is probably initiated by proteases that cleave specific sites within the propeptide, but final processing to the mature form of the active MMP that lacks the entire propeptide often requires intermolecular, autoproteolytic cleavage by the target MMP. When triggered with sulfhydryl-reactive compounds, such as organomercurials that interrupt the cysteine to Zn^{2+} coordination (*5–7*), processing of proMMPs to the active form can be entirely autoproteolytic. The physiologic activation of MMP-2 has been poorly understood, but recent evidence has shown that the MT-MMPs can initiate activation of proMMP-2 by cleaving at a specific site within the propeptide (Figs. 1 and 2) (*8, 9*). Thus far, little is known about the structural background of the cysteine-switch activation because structural work on MMPs has concentrated on isolated domains (*10*). The structure of COOH-terminally truncated proMMP-3 (stromelysin) revealed that, as predicted, the catalytic cleft is occupied by the cysteine-switch peptide (*11*). It remains unclear, however, how the rest of the propeptide contributes to the stability of the proenzyme and how limited cleavage within the propeptide can initiate the activation process.

The COOH-terminal hemopexin-like domain of MMPs is linked to the catalytic domain by a hinge peptide, and it may determine the substrate specificity of MMPs (*12*). Its structure, a four-bladed propeller around a central cavity occupied by a Ca^{2+} ion, has been determined for MMP-1, -2, and -13 (*13,14*).

Here we report the crystal structure of the full-length proform of human MMP-2 (proMMP-2). Recombinant human proMMP-2 was produced in a mutant form in which Glu^{404}, which is essential for catalytic activity of metalloproteases (*15*), was replaced by alanine. This mutant was stable against auto-

[1]Division of Matrix Biology, Department of Medical Biochemistry and Biophysics and [2]Division of Molecular Structural Biology, Department of Medical Biochemistry and Biophysics, Karolinska Institute, Stockholm, Sweden. [3]Schools of Chemistry and Biological Sciences, University of Exeter, UK.

*To whom correspondence should be addressed. E-mail: gunter@alfa.mbb.ki.se (G.S.); karl.tryggvason@mbb.ki.se (K.T.).

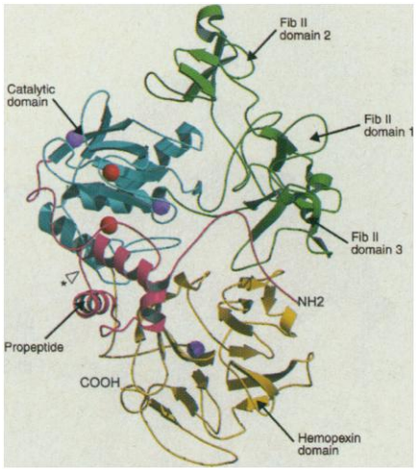

Fig. 1. Structure of proMMP-2. The prodomain, catalytic domain, fibronectin domains, and hemopexin domain are shown in red, blue, green, and yellow, respectively. Zn^{2+} ions are indicated in red, and Ca^{2+} ions are magenta (*24*). Asterisk indicates the cleavage site for MT1-MMP.

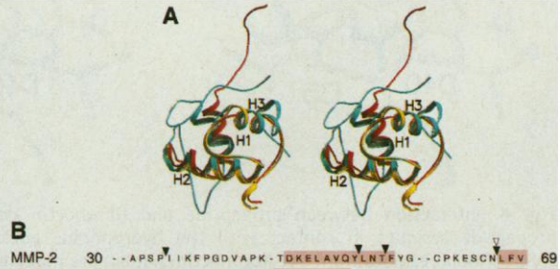

Fig. 2. Structure of the prodomain of proMMP-2 (*24*). (**A**) Comparison of the prodomains of proMMP-2 (red) and proMMP-3 (*11*) (yellow) with the noncatalytic domain of bacterial D-alanyl-D-alanyl–cleaving carboxypeptidase(blue) (*16*). (**B**) Sequence (numbering of amino acid residues is according to the SwissProt database) comparison of MMP prodomains and the NH_2-terminus of D-alanyl-D-alanyl–cleaving carboxypeptidase, with helices indicated in red. Solid arrowheads point to cleavage sites for proMMP activation (*5, 6*). Open arrowhead indicates processing site for MT-MMPs (*9*). A proteolytically sensitive region for activation of proMMP-3 (*5*) is underlined.

proteolysis and allowed the crystallization of full-length proMMP-2. We used molecular replacement (MR) techniques to determine the structure to 2.8 Å resolution (Table 1).

An overall view of proMMP-2 is shown in Fig. 1. The propeptide of proMMP-2 forms a globular domain characterized by a three-helix fold that is stabilized by hydrophobic interactions and hydrogen bonds. This structural motif is similar to the NH_2-terminal domain of D-alanyl-D-alanyl–cleaving carboxypeptidase from *Streptomyces albus* (Fig. 2A) (*16*). Comparison of the propeptide structures of proMMP-2 and proMMP-3 (*11*) shows that the cysteine-switch strand is bound into the catalytic cleft by several hydrogen bonds that are well conserved in both proMMPs. The helical part of the propeptides is similar, but the loops connecting the helices are different between proMMP-2 and proMMP-3 (*11*). The sites that get cleaved upon proteolytic activation are accommodated within these loops (Fig. 2B) (*5, 6*). MT-MMPs cleave proMMP-2 within the loop (Tyr^{58} to Asn^{66}) that connects helices H1 and H2 (Fig. 2) (*9*). This loop contains a disulfide bridge (Cys^{60} to Cys^{65}) that is unique to proMMP-2. The second loop (Phe^{81} to Ile^{94}), stabilized by two internal hydrogen bonds, is also cleaved upon autoproteolytic activation (Fig. 2). This loop is probably important for the stability of the proenzyme because it contains hydrophobic side chains that isolate the catalytic cleft and the cysteine-switch strand from solvent molecules.

The architecture of the catalytic domain, known as the matrixin fold (*17*), consists of a five-stranded β sheet and three α helices. This structure is highly conserved in MMPs and is unaffected by insertion of the fibronectin domains. The catalytic domain of proMMP-2 is similar to that of proMMP-3. The same residues form the substrate binding pockets and coordination of the catalytic Zn^{2+} ion is similar. Replacement of the charged Glu^{404} with alanine in proMMP-2 has no influence on the architecture of the active site. Also, the binding site for the structural Zn^{2+} ion is identical to a well-conserved motif found in all known MMP structures. The catalytic domain of proMMP-2 revealed one Ca^{2+} ion within the S-shaped loop and a second Ca^{2+} ion bound by two peripheral loops (Fig. 1).

The fibronectin domains of proMMP-2 (Figs. 1 and 3) are inserted between the fifth β strand and helix 2 in the catalytic domain.

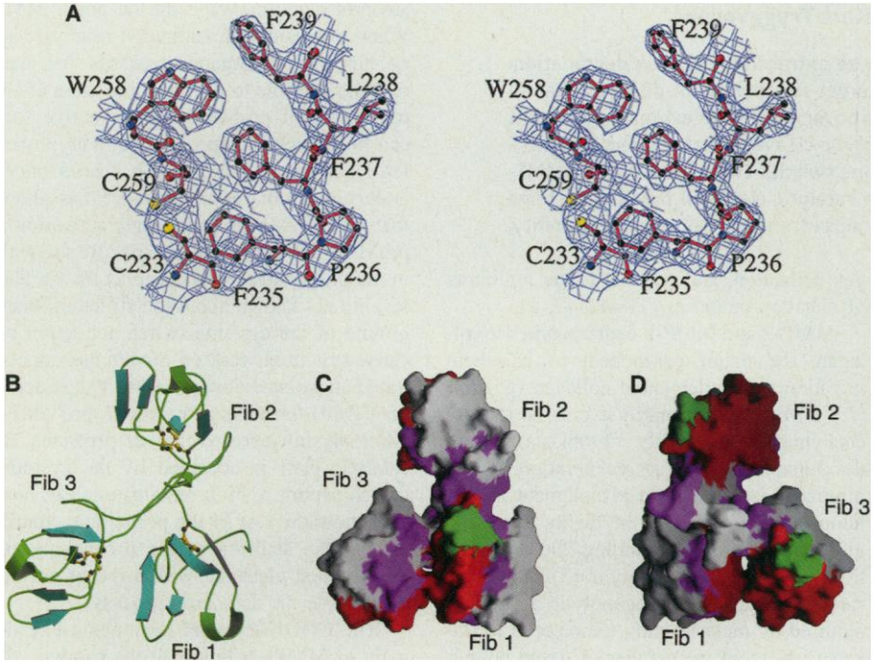

Fig. 3. Structure of fibronectin domains (*24*). **(A)** Stereoview of the electron density map contoured around cis-Pro^{236} (P236) and the Cys^{233} (C233) to Cys^{259} (C259) disulfide bridge. Sulfur atoms are yellow. **(B)** Ribbon representation showing the secondary structure with the disulfide bridges. **(C and D)** Molecular surface of the fibronectin domains show polar (green) and hydrophobic (red) residues that bind to gelatin (*19*). The orientation in (B) and (C) is the same, and the molecule in (D) is rotated by 180°. F, Phe; L, Leu; W, Trp.

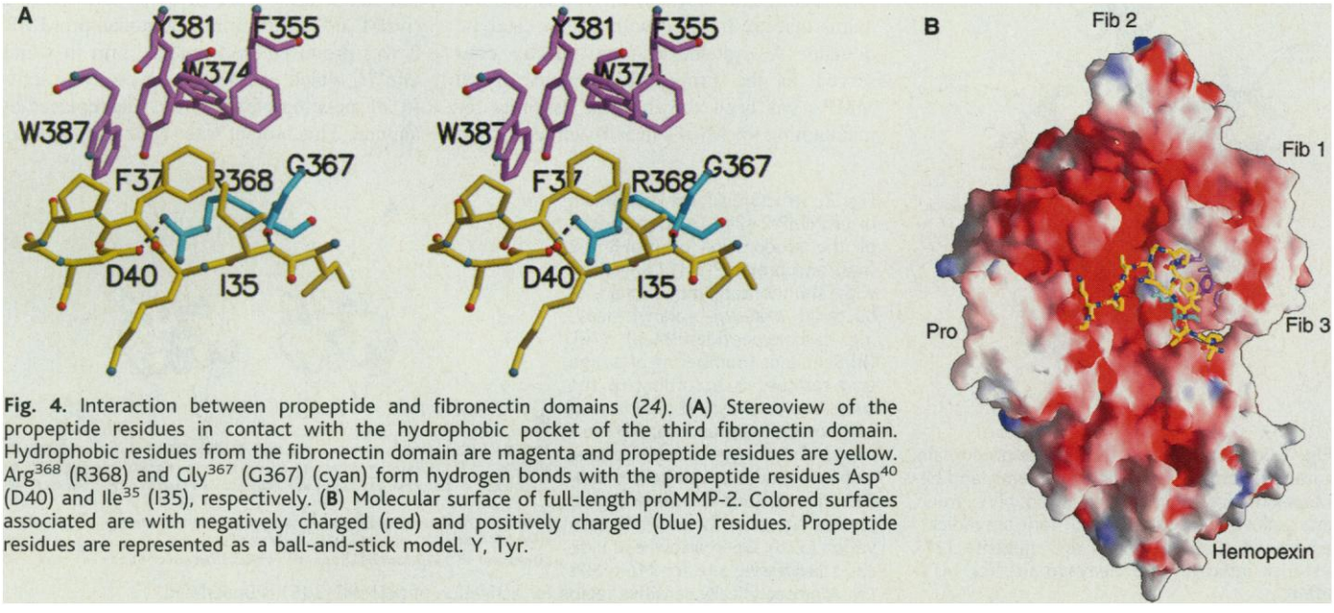

Fig. 4. Interaction between propeptide and fibronectin domains (*24*). **(A)** Stereoview of the propeptide residues in contact with the hydrophobic pocket of the third fibronectin domain. Hydrophobic residues from the fibronectin domain are magenta and propeptide residues are yellow. Arg^{368} (R368) and Gly^{367} (G367) (cyan) form hydrogen bonds with the propeptide residues Asp^{40} (D40) and Ile^{35} (I35), respectively. **(B)** Molecular surface of full-length proMMP-2. Colored surfaces associated are with negatively charged (red) and positively charged (blue) residues. Propeptide residues are represented as a ball-and-stick model. Y, Tyr.

The basic fold of the fibronectin type II-like domain (*18*) comprises a pair of β sheets, each made from two antiparallel strands, that are connected with a short α helix. The two β sheets form a hydrophobic pocket that is accessible from the outside. A cis-proline following the first β sheet is part of a hairpin turn, which orients the surrounding aromatic side chains into the hydrophobic pocket. These pockets are the structural hallmark of the fibronectin domains and probably account for substrate binding. In MMP-9, gelatin binding residues have been mapped to the hydrophobic pocket (Fig. 3) (*19*). In proMMP-2, the side chain of Phe^{37} in the propeptide inserts into the hydrophobic pocket of the third fibronectin domain (Fig. 4A). The propeptide of proMMP-2 is also bound to the third fibronectin domain by a hydrogen bond and a salt bridge (Fig. 4A). This interaction probably mimics the binding of gelatin to fibronectin type II-like domains that, based on biochemical evidence, is predicted to have all three types of interactions (*18*). The binding sites of the three fibronectin domains are not oriented toward each other to form a continuous binding motif as previously proposed (*20*). On the contrary, they turn outward as in a three-pronged fishhook (Fig. 3).

The hemopexin domain shows a four-blade propeller fold (*13,14*). The first and second propeller blades are oriented toward the catalytic domain and are linked to the first fibronectin domain by a hydrogen bond (Glu^{243} to Arg^{550}). This orientation turns propeller blades 3 and 4 away from the catalytic domain. On blades 3 and 4 are the binding sites for TIMP-2, a protein inhibitor that specifically interacts with proMMP-2 (*21*). It is unclear whether binding of TIMP-2 is the only function of the hemopexin domain in MMP-2 or whether it also modulates substrate specificity. Our structure supports the latter as the surface structure of proMMP-2 (Fig. 4B) reveals that the hemopexin domain contributes to a groove that may be involved in substrate binding.

These results provide a structural basis for understanding the activation mechanism of proMMP-2. Loops within the propeptide domain function as bait for activating proteases. Upon cleavage, the prodomain structure breaks down and its shielding of the catalytic cleft is withdrawn, allowing water to enter and hydrolyze the coordination of the cysteine to the Zn^{2+} ion.

MMPs, particularly MMP-2, have been a target for the development of antitumor therapeutics that inhibit the motility of malignant cells, a prerequisite for tumor invasion and formation of metastases. MMP inhibitors against the active site have been designed (*22*), but structural homology of their catalytic domains has made specificity a problem. The full-length proMMP-2 structure may provide alternative concepts for development of specific MMP-2 antagonists.

Table 1. Crystallographic data, phasing, and refinement. ProMMP-2 was produced as a proteolytically inactive mutant (Glu^{404} changed to Ala) with a baculovirus expression system and was purified by gelatin affinity chromatography and ion-exchange high-pressure liquid chromatography (*6*). Crystals were grown at 4°C by hanging drop crystallization. The drops contained a 1:1 mixture of protein solution (15 mg/ml) and reservoir buffer [0.2 M sodium glycine (pH 8.5) with 24 to 25% polyethylene glycol 550 monomethyl ether, 0.28 M Li_2SO_4, and 0.01 M dithiothreitol]. A heavy atom derivative was prepared by soaking the crystals in 5 mM Na_2IrCl_6. X-ray data from native and soaked crystals were collected at 100 K at beam line D2AM of the European Synchrotron Radiation Facility (ESRF, Grenoble, France) with a charge-coupled device detector and processed with the XDS software (*23*) followed by scaling and reduction with ROTAPREP and SCALA from the CCP4 package (*23*). The data showed a very high B factor and relatively strong anisotropy. An anisotropic correction was performed by SFCHECK (*23*). The crystals belonged to the tetragonal space group $I4_122$ with cell dimensions $a = b = 121.3$ Å and $c = 345.1$ Å containing one 72-kD monomer per asymmetric unit. The structure was solved by MR in combination with a single heavy atom derivative and phases were improved by multicrystal averaging. MR was conducted with AMORE (*23*) using the model of the COOH-terminal domain of gelatinase A (MMP-2) and a model containing residues 100 to 204 of porcine fibroblast collagenase (MMP-1) (*13*). The iridium site determined from a difference Fourier map was refined by MLPHARE (*23*) using the model phases. Then SIR phases were combined with the model phases by using SIGMAA (*23*). The multicrystal averaging was performed with x-ray data for the COOH-terminal domain obtained from the PDB (1GEN) using DMMULTI (*23*). The protein model was built by using O (*23*) and refined to 2.8 Å resolution, including bulk solvent correction and grouped B-factor refinement with X-PLOR (*23*) and finally with highly restrained geometries with REFMAC (*23*). The model comprises 619 amino acid residues; 2 Zn^{2+}, 3 Ca^{2+}, 1 Na^+, and 1 Cl^- ion; and 104 water molecules. No electron density was observed for the NH_2-terminal residue Ala^{30} and for residues Ser^{448} to Leu^{461} of the hinge region. rmsd, root mean square deviation. The PDB accession number for proMMP-2 is 1CK7.

Data set	Resolution (Å)	Reflections (no.)		Completeness (%)	R_{merge}* (%)	I/σ	R_{deriv}† (%)	Sites (no.)	R_{cullis}‡	Phasing power§
		Overall	Unique							
Native	34.0–2.8	333,608	32,057	99.7	11.7	20.9				
	2.9–2.8			99.7	40.2	2.0				
Na_2IrCl_6	29.0–4.5	17,019	9,476	99.9	3.5	15.6	5.6	1	0.76	1.16

Refinement statistics

Resolution shell in refinement (Å)	34.0–2.8
No. of reflections used in refinement (working set)	30,959
No. of reflections in test set	1,660
No. of nonhydrogen atoms	5,043
No. of water molecules	104
R factor (%)¶	28.6
R_{free} factor (%)‖	32.7
rmsd bond length (Å)	0.012
rmsd bond angle (°)	2.4
Average B factor (Å^2)	63.5
rmsd B (Å^2)	1.7
Ramachandran plot	
Residues in the most favorable region (%)	88.5
Nonglycine residues in disallowed regions (%)	0.0

*$R_{merge} = \Sigma_h\Sigma_i|I(h)_i - \langle I(h)\rangle|/\Sigma_h\Sigma_i I(h)_i$, where $I(h)_i$ is the ith measurement. †$R_{deriv} = \Sigma||F_{PH}| - |F_P||/\Sigma|_{PH}|$, where F_{PH} and F_P are protein and heavy-atom derivative structure factors, respectively. ‡$R_{cullis} = \Sigma||F_{PH} - F_P| - F_{H(calc)}|/\Sigma|F_{PH} - F_P|$, where F_{PH} and F_P are as defined above and $F_{H(calc)}$ is the calculated heavy-atom structure factor (only for centric reflections). §Phasing power $= [\Sigma|F_{PH(calc)}|^2/\Sigma|F_{PH(obs)} - F_{P(calc)}|^2]^{1/2}$, where $|F_{PH(obs)} - F_{P(calc)}|$ is the lack of closure error to maximum resolution indicated. ¶R factor $= \Sigma||F_O| - |F_C||/\Sigma|F_O|$, where F_O and F_C are the observed and calculated structure factors, respectively. ‖R_{free} is calculated over reflections in a test set not included in the refinement.

References and Notes

1. C. B. Basbaum and Z. Werb, *Curr. Opin. Cell Biol.* **8**, 731 (1996); E. C. Kohn and L. A. Liotta, *Cancer Res.* **55**, 1856 (1995).
2. H. Birkedal-Hansen, *Curr. Opin. Cell Biol.* **7**, 728 (1995)); I. Massova, L. P, Kotra, R. Fridman, S. Mobashery, *FASEB J.* **12**, 1075 (1998).
3. T. Salo, L. A. Liotta, K. Tryggvason, *J. Biol. Chem.* **258**, 3058 (1983); P. Reponen *et al.*, *ibid.* **267**, 7856 (1992); C. Pyke *et al.*, *Cancer Res.* **52**, 1336 (1992).
4. H. E. Van Wart and H. Birkedal-Hansen, *Proc. Natl. Acad. Sci. U.S.A.* **87**, 5578 (1990).
5. H. Nagase, J. J. Enghild, K. Suzuki, G. Salvesen, *Biochemistry* **29**, 5783 (1990).
6. U. Bergmann, A. Tuuttila, W. G. Stetler-Stevenson, K. Tryggvason, *ibid.* **34**, 2819 (1995).
7. T. Crabbe, C. Ioannou, A. J. Docherty, *Eur. J. Biochem.* **218**, 431 (1993); S. J. Atkinson *et al.*, *J. Biol. Chem.* **270**, 30479 (1995).
8. H. Sato *et al.*, *Nature* **370**, 61 (1994).
9. A. Y. Strongin, B. L. Marmer, G. A. Grant, G. I. Goldberg, *J. Biol. Chem* **268**, 14033 (1993); H. Will, S. J. Atkinson, G. S. Butler, B. Smith, G. Murphy, *ibid.* **271**, 17119 (1996).
10. B. Lovejoy *et al.*, *Science* **263**, 375 (1994); P. R. Gooley *et al.*, *Nature Struct. Biol.* **1**, 111 (1994); M. F. Browner, W. W. Smith, A. L. Castelhano, *Biochemistry* **34**, 6602 (1995); T. Stams *et al.*, *Nature Struct. Biol.* **1**, 119 (1994).
11. J. W. Becker *et al.*, *Protein Sci.* **4**, 1966 (1995).
12. G. Murphy *et al.*, *J . Biol. Chem.* **267**, 9612 (1992); U. M. Wallon and C. M. Overall, *ibid.* **272**, 7473 (1997).
13. J. Li *et al.*, *Structure* **3**, 541 (1995).
14. A. M. Libson *et al.*, *Nature Struct. Biol.* **2**, 938 (1995); U. Gohlke *et al.*, *FEBS Lett.* **378**, 126 (1996); F. X. Gomis-Ruth *et al.*, *J. Mol. Biol.* **264**, 556 (1996).

15. D. G. Hangauer, A. F. Monzingo, B. W. Matthews, *Biochemistry* **23**, 5730 (1984).
16. O. Dideberg *et al.*, *Nature* **299**, 469 (1982); J. M. Ghuysen, J. Lamotte-Brasseur, B. Joris, G. D. Shockman, *FEBS Lett.* **342**, 23 (1994).
17. W. Stocker and W. Bode, *Curr. Opin. Struct. Biol.* **5**, 383 (1995).
18. K. L. Constantine *et al.*, *J. Mol. Biol.* **223**, 281 (1992); A. R. Pickford, J. R. Potts, J. R. Bright, I. Phan, I. D. Campbell, *Structure* **5**, 359 (1997).
19. I. E. Collier, P. A. Krasnov, A. Y. Strongin, H. Birkedal-Hansen, G. I. Goldberg, *J. Biol. Chem.* **267**, 6776 (1992).
20. L. Bányai, H. Tordai, L. Patthy, *ibid.* **271**, 12003 (1996).
21. F. Willenbrock *et al.*, *Biochemistry* **32**, 4330 (1993); M. W. Olson, D. C. Gervasi, S. Mobashery, R. Fridman, *J. Biol. Chem.* **272**, 29975 (1997); C. M. Overall *et al.*, *ibid.* **274**, 4421 (1999).
22. J. Hodgson, *Biotechnology* **13**, 554 (1995); A. E. Yu, R. E. Hewitt, E. W. Connor, W. G. Stetler-Stevenson, *Drugs Aging* **11**, 229 (1997); S. A. Watson and G. Tierney, *Biodrugs* **9**, 325 (1998).
23. XDS [W. Kabsch, *J. Appl. Crystallogr.* **21**, 916 (1988)]; CCP4 programs [CCP4, Collaborative Computational Project No. 4, Daresbury, UK, *Acta Crystallogr.* D **50**, 760 (1994)]; SFCHECK [A. A. Vagin, J. Richelle, S. J. Wodak, *ibid.* **55**, 191 (1999)]; AMORE [J. Navaza, *Acta Crystallogr.* A **50**, 157 (1994)]; O [T. A. Jones, J.-Y. Zou, S. W. Cowan, M. Kjeldgaard, *ibid.* **47**, 110 (1991)]; and X-PLOR [A. T. Brünger, *X-PLOR, Version 3.1: A System for X-Ray Crystallography and NMR* (Yale Univ. Press, New Haven, CT, 1992)].
24. Figures 1, 2A, 3, A and B, and 4A were made with MOLSCRIPT [P. J. Kraulis, *J. Appl. Crystallogr.* **24**, 946 (1991)] and RASTER3D [E. A. Merrit and M. E. P. Murphy, *Acta Crystallogr.* D **50**, 869 (1994)]. Figures 3, C and D, and 4B were made with GRASP [A. Nichols, K. A. Sharp, B. Honig, *Proteins* **11**, 281 (1991)].
25. Supported by grants from the Swedish Cancer Foundation, EC project BMH4-CT 96-0012, Novo Nordisk Foundation, and Hedlund's Foundation. We thank Tiina Berg, Ilkka Miinalainen, and Kristian Tryggvason for technical assistance with insect cell cultures. We are also grateful to Richard Kahn and Tatjana Sandalova for assistance with the data collection. Beam time was provided by the ESRF.

21 December 1998; accepted 28 April 1999

Genetics of Mouse Behavior: Interactions with Laboratory Environment

John C. Crabbe,[1]* Douglas Wahlsten,[2] Bruce C. Dudek[3]

Strains of mice that show characteristic patterns of behavior are critical for research in neurobehavioral genetics. Possible confounding influences of the laboratory environment were studied in several inbred strains and one null mutant by simultaneous testing in three laboratories on a battery of six behaviors. Apparatus, test protocols, and many environmental variables were rigorously equated. Strains differed markedly in all behaviors, and despite standardization, there were systematic differences in behavior across labs. For some tests, the magnitude of genetic differences depended upon the specific testing lab. Thus, experiments characterizing mutants may yield results that are idiosyncratic to a particular laboratory.

Targeted and chemically induced mutations in mice are valuable tools in biomedical research, especially in the neurosciences and psychopharmacology. Phenotypic effects of a knockout often depend on the genetic background of the mouse strain carrying the mutation (*1*), but the effects of environmental background are not generally known.

Different laboratories commonly employ their own idiosyncratic versions of behavioral test apparatus and protocols, and any laboratory environment also has many unique features. These variations have sometimes led to discrepancies in the outcomes reported by different labs testing the same genotypes for ostensibly the same behaviors (*2*). Previous studies could not distinguish between interactions arising from variations in the test situation itself and those arising from subtle environmental differences among labs. Usually, such differences are eventually resolved by repetition of tests in multiple labs. However, null mutants and transgenic mice are often scarce and tend to be behaviorally characterized in a single laboratory with a limited array of available tests.

We addressed this problem by testing six mouse behaviors simultaneously in three laboratories (Albany, New York; Edmonton, Alberta, Canada; and Portland, Oregon) using exactly the same inbred strains and one null mutant strain (*3*). We went to extraordinary lengths to equate test apparatus, testing protocols, and all possible features of animal husbandry (*4*). One potentially important feature was varied systematically. Because many believe that mice tested after shipping from a supplier behave differently from those reared in-house, we compared mice either shipped or bred locally at the same age (77 days) starting at the same time (0830 to 0900 hours local time on 20 April 1998) in all three labs (*5*). Each mouse was given the same order of tests [Day 1: locomotor activity in an open field; Day 2: an anxiety test, exploration of two enclosed and two open arms of an elevated plus maze; Day 3: walking and balancing on a rotating rod; Day 4: learning to swim to a visible platform; Day 5: locomotor activation after cocaine injection; Days 6 to 11: preference for drinking ethanol versus tap water (*6*)].

Despite our efforts to equate laboratory environments, significant and, in some cases, large effects of site were found for nearly all variables (Table 1). Furthermore, the pattern of strain differences varied substantially among the sites for several tests. Sex differ-

Table 1. Statistical significance and effect sizes for selected variables in the multisite trial. Color of cell depicts Type I error probability or significance of main effects and two-way interactions from 8 × 2 × 3 × 2 analyses of variance: blue, $P < 0.00001$; purple, $P < 0.001$; gold, $P < 0.01$; dashes with no shading, $P > 0.01$. Cell entries are effect sizes, expressed as partial omega squared, the proportion of variance accounted for by the factor or interaction if only that factor were in the experimental design (range = 0 to 1.0). Multiple R^2 (unbiased estimate) gives the proportion of the variance accounted for by all factors. For the water escape task, results are based on only seven strains because most A/J mice never escaped because of wall-hugging. We recognize that the issue of appropriate alpha level correction for multiple comparisons is contentious. Details of the statistical analyses are available on the Web site (*4*), including a discussion of our rationale for presenting uncorrected values in this table.

Task	Measure	Eight Genotypes	Three Sites	Two Sexes	Local vs Shipped	Genotype x Site	Genotype x Sex	Genotype x Ship	Multiple R^2
Open field	Distance in 15 min	.600	.157	----	----	.059	.045	----	.604
Open field	# vertical movements	.788	.281	.039	----	----	----	----	.772
Cocaine	Difference from Day 1	.338	.052	----	----	.026	----	----	.342
Plus maze	Total arm entries	.385	.327	----	----	.210	----	----	.660
Plus maze	Time in open arms	.092	.212	----	----	.066	----	----	.266
Water maze	Mean escape latency	.221	----	----	.026	----	----	----	.177
Alcohol preference	Alcohol consumed (g/kg)	.483	----	.043	----	----	----	----	.451
Body size	Weight (g)	.408	.204	.637	----	.071	.070	----	.698

[1]Portland Alcohol Research Center, Department of Veterans Affairs Medical Center and Department of Behavioral Neuroscience, Oregon Health Sciences University, Portland, OR 97201, USA. [2]Department of Psychology, University of Alberta, Edmonton, Alberta, Canada T6G 2E9. [3]Department of Psychology, State University of New York at Albany, Albany, NY 12222, USA.

*To whom correspondence should be addressed. E-mail: crabbe@ohsu.edu